Analysis of resonant inelastic x-ray scattering at the *K* edge in NiO

Manabu Takahashi,[1] Jun-Ichi Igarashi,[2] and Takuji Nomura[3]
[1]*Faculty of Engineering, Gunma University, Kiryu, Gunma 376-8515, Japan*
[2]*Faculty of Science, Ibaraki University, Mito, Ibaraki 310-8512, Japan*
[3]*Synchrotron Radiation Research Center, Japan Atomic Energy Agency, Hyogo 679-5148, Japan*
(Received 12 November 2006; revised manuscript received 9 February 2007; published 19 June 2007)

We analyze the resonant inelastic x-ray scattering (RIXS) spectra at the Ni *K* edge in an antiferromagnetic insulator NiO by applying the theory developed by the present authors. It is based on the Keldysh-Green function formalism, and treats the core-hole potential in the intermediate state within the Born approximation. We calculate the single-particle energy bands within the Hartree-Fock approximation on the basis of the multiorbital tight-binding model. Using these energy bands together with the 4*p* density of states from an *ab initio* band-structure calculation, we calculate the RIXS intensities as a function of energy loss. By taking account of electron correlation within the random-phase approximation (RPA), we obtain quantitative agreement with the experimental RIXS spectra, which consist of two prominent peaks around 5 and 8 eV, and the former shows considerable dispersion, while the latter shows no dispersion. We interpret the peaks as a result of a band-to-band transition augmented by the RPA correlation.

DOI: 10.1103/PhysRevB.75.235113 PACS number(s): 78.70.Ck, 71.20.Be, 71.28.+d, 78.20.Bh

I. INTRODUCTION

Excitations in solids are fundamental to describe physical properties, such as the response to external perturbations and temperature dependence. They may be characterized into two types, spin and charge excitations. For the former, the inelastic neutron scattering is quite powerful to investigate the energy-momentum relations. By contrast, charge excitations have been investigated by measuring the optical conductivity, but the momentum transfer is limited to nearly zero.[1] The electron energy loss spectroscopy can detect the momentum dependence of charge excitations, but it suffers from strong multiple scattering effects.[2] Recently, taking advantage of strong synchrotron sources, the resonant inelastic x-ray scattering (RIXS) has become a powerful tool to probe charge excitations in solids.[3–9] In transition-metal compounds, *K*-edge resonances are widely used to observe momentum dependence, because corresponding x rays have wavelengths of the same order of lattice spacing. The process is described as a second-order optical process that a 1*s* core electron is prompted to an empty 4*p* state by absorbing photon, then charge excitations are created in order to screen the core-hole potential, and finally the photoexcited 4*p* electron is recombined with the core hole by emitting photon. In the end, charge excitations are left with energy and momentum transferred from photon. In cuprates, the RIXS spectra are found to have clear momentum dependence.[5,6,9]

For NiO, a Ni *K*-edge RIXS experiment has been carried out by Kao *et al.*, in which the spectral peaks were not well resolved, and had no clear momentum dependence, probably due to the experimental resolution.[3] Recently, a *K*-edge RIXS experiment has been carried out at Taiwan beamline in Spring-8.[10] They have observed the spectra as a function of energy loss by tuning the incident photon energy at 8351 eV, which corresponds to the Ni *K*-edge absorption peak. The observed spectra consist of two prominent peaks at 5 and 8 eV, and the 5 eV peak considerably changes while the 8 eV peak does not change with changing momenta. In addition, extra tiny peaks are found below 4 eV, which are called *d-d* excitation. In this paper, we analyze the RIXS spectra for NiO by developing the formalism of Nomura and Igarashi.[11,12] This theory is based on the many-body formalism of Keldysh, and is regarded as an extension of the resonant Raman theory developed by Nozières and Abrahams.[13] The core-hole potential is treated within the Born approximation. Higher-order effects beyond the Born approximation have been evaluated on the *K*-edge RIXS in La_2CuO_4.[14] Although the core-hole potential is rather strong, the higher-order effects are found to cause only minor change in the spectral shape.[14] In this situation, the RIXS spectra can be connected to the 3*d*-density-density correlation function in the equilibrium state. We develop the formalism by clarifying the equivalence of the Keldysh formalism and the conventional Green's function formalism and by deriving the RIXS formula for possible bound states corresponding to the *d-d* excitations. Advantages of the present formalism are, in contrast to the numerical diagonalization method, as follows: it is applicable to three-dimensional models consisting of many orbitals, and it provides clear physical interpretation.

We construct a detailed multiorbital tight-binding model including all 3*d* orbitals, as well as the full intra-atomic Coulomb interaction between 3*d* orbitals. Applying the Hartree-Fock approximation (HFA) to the model, we obtain the antiferromagnetic (AF) solution with an appropriate description of the single-particle spectra having a large energy gap. Unoccupied 3*d* states on a Ni site consist of minority spin states on the site and have almost the e_g character. Note that the band calculation with the local-density approximation (LDA) fails to reproduce the energy gap of 4 eV. The RIXS spectra are interpreted as a result of a band-to-band transition to screen the 1*s* core hole. Therefore, the transition occurs through the amplitude of the e_g character. Treating electron correlations by the random-phase approximation (RPA), we find that spectral shape as a function of energy loss is strongly modified in the continuum spectra. In order to obtain quantitative agreement with the experiment, we need to take account of the RPA correlation. Note that the same

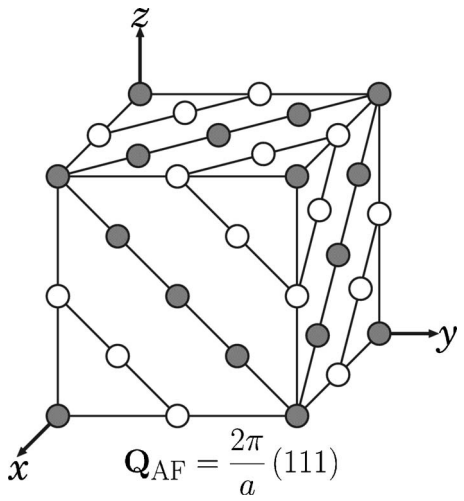

FIG. 1. Schematic view of a NiO crystal with type-II AF order. Only Ni atoms are shown. Wave vector $\mathbf{Q}_{\mathrm{AF}}$ characterizes the AF modulation. The direction of magnetic moment on the Ni site denoted by filled circle is antiparallel to that on the site denoted by open circle.

analysis of the RIXS in cuprates has been successful to reproduce the experimental spectra. The success of the analysis for NiO would add another evidence of the usefulness of the present scheme of analyzing the RIXS spectra.

The present formalism describes the *d-d* excitation by the bound state in the density-density correlation function. We obtain bound states but with extremely small intensities in comparison with the experiment.

The present paper is organized as follows. In Sec. II, we study the electronic structure on the basis of the band calculation, and then introduce a multiorbital tight-binding model. We calculate the single-particle Green's function within the HFA in the AF phase of NiO. In Sec. III, we summarize the formula for the RIXS spectra, including the discussion of the bound states. In Sec. IV, we calculate the RIXS spectra by taking account of the RPA correction in comparison with the experiment. Section V is devoted to the concluding remarks.

II. ELECTRONIC STRUCTURE OF NICKEL OXIDE

The crystal structure of NiO is NaCl type with lattice constant $a=4.177$ Å. Ni atoms form a fcc lattice, as shown in Fig. 1. Type-II AF order develops below $T_N=523$ K. The order parameter is characterized by a wave vector directing to one of four-body diagonals in the fcc lattice.[15]

A. *Ab initio* calculation

We calculate the electronic band structure using the muffin-tin Korringa-Kohn-Rostoker (KKR) method within the LDA. Although we obtain a stable AF self-consistent solution, we have the energy gap 0.2 eV, which is much smaller than the experimental one, ~4.3 eV.[16] Figure 2 shows the calculated density of states (DOS) projected onto Ni 3*d* and O 2*p* states. The difference between the calculation and the experiment in the energy gap may be improved by using the so-called LDA+*U* method, which is a hybrid of

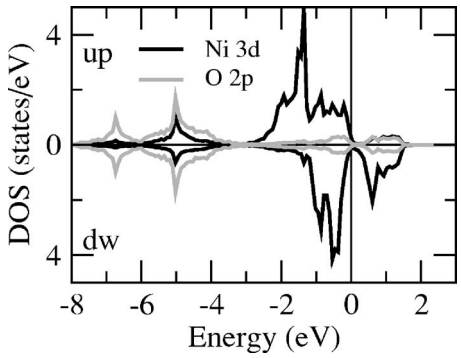

FIG. 2. Density of states projected onto Ni 3*d* and O 2*p* states calculated within the LDA. The energy zero is at the top of the valence band.

the LDA and the HFA for the Coulomb interaction in the Ni 3*d* orbitals. Since we need to calculate the two-particle correlation function within the RPA, we introduce a multiorbital tight-binding model in place of the *ab initio* calculation, and apply the RPA in the following.

In contrast to the failure for the Ni 3*d* states, we expect that the Ni 4*p* states are well described within the LDA, since the 4*p* band has a wide width ≳20 eV and thereby are weakly correlated. We show the 4*p* DOS convoluted with the Lorentzian function with the full width of half maximum (FWHM) 2 eV in Fig. 3. The FWHM corresponds to the core-hole lifetime width. The calculated curve agrees fairly well with the experimental one.

B. Multiorbital tight-binding model

We introduce a multiorbital tight-binding model defined by

$$H = H_0 + H_I, \tag{1}$$

$$\begin{aligned} H_0 = & \sum_{im\sigma} E^d n^d_{im\sigma} + \sum_{j\ell\sigma} E^p n^p_{j\ell\sigma} + \sum_{\langle i,j\rangle} \sum_{\sigma\ell m} (t^{dp}_{im,j\ell} d^\dagger_{im\sigma} p_{j\ell\sigma} + \text{H.c.}) \\ & + \sum_{\langle j,j'\rangle} \sum_{\sigma\ell\ell'} (t^{pp}_{j\ell,j'\ell'} p^\dagger_{j\ell\sigma} p_{j'\ell'\sigma} + \text{H.c.}) \\ & + \sum_{\langle i,i'\rangle} \sum_{\sigma mm'} (t^{dd}_{im,i'm'} d^\dagger_{im\sigma} d_{i'm'\sigma} + \text{H.c.}), \end{aligned} \tag{2}$$

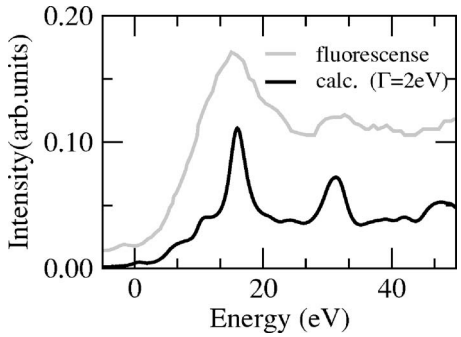

FIG. 3. Density of states projected onto Ni 4*p* states calculated within the LDA. The experimental curve is taken from Fig. 4 in Ref. 17

TABLE I. Parameter values for the tight-binding model of NiO in units of eV.

	SK param.		Slater integral	
Ni	$dd\sigma$	−0.227	F^0	5.00
	$dd\pi$	−0.103	F^2	10.57
	$dd\delta$	−0.010	F^4	7.56
Ni-O	$pd\pi$	−1.400	Charge-transfer energy	
	$pd\sigma$	0.630	Δ	4.5
O	$pp\sigma$	0.600		
	$pp\pi$	−0.150		

$$H_I = \frac{1}{2}\sum_i \sum_{\nu_1\nu_2\nu_3\nu_4} g(\nu_1\nu_2;\nu_3\nu_4) d^\dagger_{i\nu_1} d^\dagger_{i\nu_2} d_{i\nu_4} d_{i\nu_3}. \quad (3)$$

The part H_0 represents the kinetic energy, where $d_{im\sigma}$ and $p_{j\ell\sigma}$ denote the annihilation operators of an electron with spin σ in the $3d$ orbit m of Ni site i and of an electron with spin σ in the $2p$ orbit ℓ of the O site j, respectively. Number operators $n^d_{im\sigma}$ and $n^p_{j\ell\sigma}$ are defined by $n^d_{im\sigma}=d^\dagger_{im\sigma}d_{im\sigma}$, $n^p_{j\ell\sigma}=p^\dagger_{j\ell\sigma}p_{j\ell\sigma}$. The transfer integrals, $t^{dp}_{im,j\ell}$, $t^{pp}_{j\ell,j'\ell'}$, $t^{dd}_{im,i'm'}$, are evaluated from the Slater-Koster two-center integrals, $(pd\sigma)$, $(pd\pi)$, $(pp\sigma)$, $(pp\pi)$, $(dd\sigma)$, $(dd\pi)$, $(dd\delta)$.[18] The d-level position relative to the p levels is given by the charge-transfer energy Δ defined by $\Delta=E_d-E_p+8U$ for the d^8 configuration.[19] Here, U is the multiplet-averaged d-d Coulomb interaction given by $U=F^0-(2/63)F^2-(2/63)F^4$, where F^0, F^2, and F^4 are Slater integrals for $3d$ orbitals. The part H_I represents the intra-atomic Coulomb interaction on transition metal sites. The Coulomb interaction on O sites is neglected. The interaction matrix element $g(\nu_1\nu_2;\nu_3\nu_4)$ is written in terms of F^0, F^2, and F^4 [ν stands for (m,σ)].

We determine most parameter values from a cluster-model analysis of photoemission spectra.[20] The values for $(dd\sigma)$, $(dd\pi)$, and $(dd\delta)$ cannot be determined from the cluster-model analysis, and, therefore, we set them close to Mattheiss' LDA estimates.[21] Among Slater integrals, F^2 and F^4 are known to be slightly screened by solid-state effects, so that we use the values multiplying 0.8 to atomic values. On the other hand, F^0 is known to be considerably screened, so that we regard the value as an adjustable parameter to get a reasonable band gap. Table I lists the parameter values used in the present calculation.

C. Hartree-Fock approximation

For the AF order shown in Fig. 1, a unit cell contains two Ni atoms and two O atoms. We allocate variable λ with $\lambda=1,2$ for Ni and $\lambda=3,4$ for O to distinguish atoms in the unit cell. Labeling a unit cell by n, we introduce annihilation operators $A_{\lambda m\sigma}(n)$, which is $d_{im\sigma}(n)$ for $\lambda=1,2$ and $p_{jm\sigma}(n)$ for $\lambda=3,4$. The Fourier transform is defined in the magnetic Brillouin zone (BZ),

$$A_{\mathbf{k}\lambda m\sigma} = \sqrt{\frac{2}{N}}\sum_n A_{\lambda m\sigma}(n) e^{i\mathbf{k}\cdot\mathbf{r}_n}, \quad (4)$$

where $\mathbf{r}_n$ represents a position vector of the unit cell, and n runs over $N/2$ unit cells. Note that a single phase factor $\mathbf{k}\cdot\mathbf{r}_n$ is applied to all the states in each unit cell. This definition of the Fourier transform is slightly different from our previous papers,[12,14] in which each atom has a phase factor $\mathbf{k}\cdot\mathbf{r}_i$ with $\mathbf{r}_i$ being the position vector of each atom. With these operators, the single-particle Green's function is introduced in a matrix form,

$$[\hat{G}(\mathbf{k},\omega)]_{\mu\mu'} = -i\int \langle T(A_{\mathbf{k}\mu}(t)A^\dagger_{\mathbf{k}\mu'}(0))\rangle e^{i\omega t}dt, \quad (5)$$

where T is the time ordering operator and μ is the abbreviation of $(\lambda m\sigma)$.

In the HFA, we disregard the fluctuation terms in H_I and approximate H_I by

$$H_I^{HF} = \frac{1}{2}\sum_i \sum_{\nu_1\nu_2\nu_3\nu_4} \Gamma^{(0)}(\nu_1\nu_2;\nu_3\nu_4)\langle d^\dagger_{i\nu_2} d_{i\nu_3}\rangle d^\dagger_{i\nu_1} d_{i\nu_4}, \quad (6)$$

where $\Gamma^{(0)}$ is the antisymmetric vertex function defined by

$$\Gamma^{(0)}(\nu_1\nu_2;\nu_3\nu_4) = g(\nu_1\nu_2;\nu_3\nu_4) - g(\nu_1\nu_2;\nu_4\nu_3), \quad (7)$$

with ν being the abbreviation of $(m\sigma)$ and i running over all Ni sites. The $\langle X\rangle$ denotes the ground-state average of the operator X. Considering the equation of motion with the Hamiltonian $H_0+H_I^{HF}$, we obtain

$$(\omega\hat{I} - \hat{J}(\mathbf{k}))\hat{G}(\mathbf{k},\omega) = \hat{I}, \quad (8)$$

where $\hat{I}$ is the unit matrix, and $\hat{J}(\mathbf{k})$ is defined through the relation

$$[H_0 + H_I^{HF}, A_{\mathbf{k}\mu}] = \sum_{\mu'} [\hat{J}(\mathbf{k})]_{\mu\mu'} A_{\mathbf{k}\mu'}. \quad (9)$$

Introducing a unitary matrix $\hat{U}(\mathbf{k})$ to diagonalize $\hat{J}(\mathbf{k})$, that is, $[\hat{U}(\mathbf{k})^{-1}\hat{J}(\mathbf{k})\hat{U}(\mathbf{k})]_{jj'}=E_j(\mathbf{k})\delta_{jj'}$, we express the Green's function as

$$\hat{G}(\mathbf{k},\omega) = \hat{U}(\mathbf{k})\hat{D}(\mathbf{k},\omega)\hat{U}(\mathbf{k})^{-1}, \quad (10)$$

with

$$[\hat{D}(\mathbf{k},\omega)]_{jj'} = \frac{1}{\omega - E_j(\mathbf{k}) + i\delta\,\mathrm{sign}(E_j(\mathbf{k})-\mu_0)}\delta_{jj'}, \quad (11)$$

where μ_0 is the chemical potential. Here j and j' denote energy eigenstates. The $\hat{J}(\mathbf{k})$ contains the expectation values of the $3d$ electron density on the ground state. Noting that Ni atoms in a unit cell correspond to $\lambda=1,2$, the self-consistent equation is given by

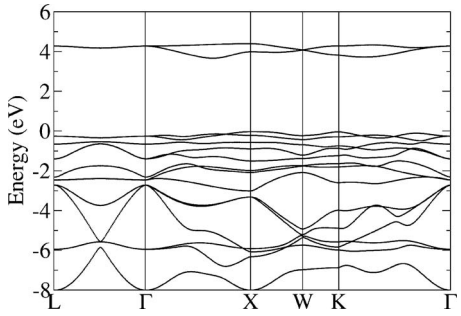

FIG. 4. Energy band as a function of momentum along symmetry lines within the HFA. The energy zero is at the top of the valence band.

$$\langle A^{\dagger}_{\lambda m\sigma} A_{\lambda m'\sigma'}\rangle = \frac{2}{N}\sum_{\mathbf{k}} (-i)\int [\hat{G}(\mathbf{k},\omega)]_{\lambda m'\sigma,\lambda m\sigma} \times e^{i\omega 0^+}\frac{d\omega}{2\pi} \quad \text{for } \lambda = 1,2. \tag{12}$$

Only the diagonal parts are nonvanishing, if $3d$ orbitals are specified by $m=xy$, yz, zx, x^2-y^2, $3z^2-r^2$ with x, y, z referring to the crystal axes, that is, $\langle d^{\dagger}_{jm\sigma} d_{jm'\sigma}\rangle \neq 0$ only for $m=m'$.

A stable self-consistent solution exists for the AF order shown in Fig. 1. Figure 4 shows the energy band as a function of momentum along symmetry lines. The F^0 value of 5 eV leads to the energy gap ~4 eV, which is consistent with the experiment.

Figures 5 and 6 show the DOS projected onto Ni $3d$ and O $2p$ states, and the $3d$ DOS divided into the e_g and t_{2g} characters, respectively. The states around the top of the valence band have relatively large weights of O $2p$ state, implying that NiO is an insulator of charge-transfer type. Regarding the majority spin states, the $3d$ states are almost fully occupied; the e_g character is concentrated around the top and bottom of the valence band, while the t_{2g} character is around the middle of the valence band. Regarding the minority spin states, the unoccupied states have almost the e_g character. The t_{2g} character dominates around the top of the valence band, while the e_g character is widely distributed with relative small weight.

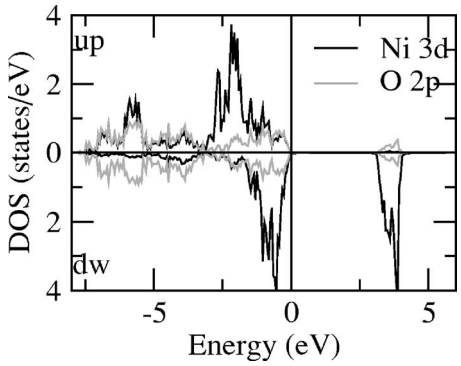

FIG. 5. Spin-resolved DOS projected onto Ni $3d$ states and onto O $2p$ states. The energy zero is at the top of the valence band.

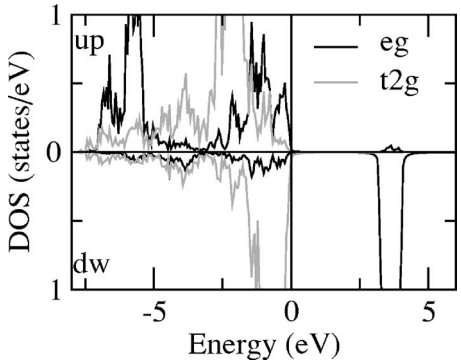

FIG. 6. Spin-resolved DOS divided into the t_{2g} and e_g characters. The energy zero is at the top of the valence band.

III. FORMULA FOR RIXS SPECTRA

A. General expression

We summarize a general expression for RIXS spectra following the papers of Nomura and Igarashi.[12] See Ref. 14 for the detailed derivation.

For the interaction between photon and matter, we consider the dipole transition at the K edge, where the $1s$ core electron is excited to the $4p$ band with absorbing photon and the reverse process takes place. This process may be described by

$$H_x = w\sum_{\mathbf{q}\alpha}\frac{1}{\sqrt{2\omega_{\mathbf{q}}}}\sum_{i\eta\sigma} e^{(\alpha)}_{\eta} p'^{\dagger}_{i\eta\sigma} s_{i\sigma} c_{\mathbf{q}\alpha} e^{i\mathbf{q}\cdot\mathbf{r}_i} + \text{H.c.}, \tag{13}$$

where w represents the matrix element of the $1s\rightarrow 4p$ dipole transition. It is approximated as a constant, since the $1s$ state is well localized. The $e^{(\alpha)}_{\eta}$ represents the ηth component ($\eta=x,y,z$) of two kinds of polarization vectors ($\alpha=1,2$) of photon. Annihilation operators $p'_{i\eta\sigma}$ and $s_{i\sigma}$ are for states $4p_{\eta}$ and state $1s$ at Ni site i, respectively. The annihilation operator $c_{\mathbf{q}\alpha}$ is for photon with momentum $\mathbf{q}$ and polarization α. In the momentum representation, the Hamiltonians for the core electron and for the $4p$ electron are given by

$$H_{1s} = \epsilon_{1s}\sum_{\mathbf{k}\sigma} s^{\dagger}_{\mathbf{k}\sigma} s_{\mathbf{k}\sigma}, \tag{14}$$

$$H_{4p} = \sum_{\mathbf{k}\eta\sigma} \epsilon^{\eta}_{4p}(\mathbf{k}) p'^{\dagger}_{\mathbf{k}\eta\sigma} p'_{\mathbf{k}\eta\sigma}. \tag{15}$$

The photocreated $1s$ core hole induces charge excitations through the attractive core-hole potential, which may be described by

$$H_{1s\text{-}3d} = V\sum_{im\sigma\sigma'} d^{\dagger}_{im\sigma} d_{im\sigma} s^{\dagger}_{i\sigma'} s_{i\sigma'}, \tag{16}$$

where i runs over Ni sites, and V may be 5–10 eV in NiO.

The above process is diagrammatically represented in Fig. 7 on the basis of the Keldysh-Green function scheme.[22] The upper half belongs to the outward time leg and the bottom part to the backward time leg. The core-hole potential works at time τ in the outward time leg and at time τ' in the backward time leg. The Born approximation is utilized to the

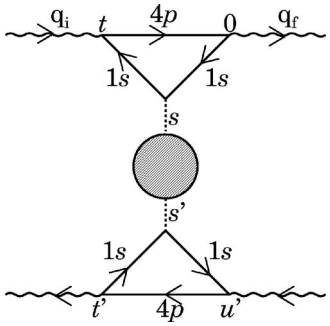

FIG. 7. Diagrams for the RIXS intensity within the Born approximation to the $1s$ core-hole potential. The solid lines with $4p$ and $1s$ represent the bare Green's functions for the $4p$ electron and the $1s$ core electron. The dotted lines represent the core-hole potential V. The shaded part represents the Keldysh-type Green's function, which connects the outward time leg on the top half and the backward time leg on the bottom half.

core-hole potential. The shaded part, connecting the outward and backward time legs, represents the Keldysh-type Green's function,

$$Y^{+-}_{\xi',\xi}(\mathbf{q},\tau'-\tau) = \int Y^{+-}_{\xi',\xi}(\mathbf{q},\omega)e^{-i\omega(\tau'-\tau)}\frac{d\omega}{2\pi} \tag{17}$$

$$= \langle (\rho_{\mathbf{q}\lambda' m'\sigma'})^{\dagger}(\tau')\rho_{\mathbf{q}\lambda m\sigma}(\tau)\rangle, \tag{18}$$

where abbreviations $\xi=(\lambda m\sigma)$, $\xi'=(\lambda' m'\sigma')$ are used with $\lambda=1,2$, $\lambda'=1,2$ in Eq. (17), for emphasizing the variables are for Ni atoms. The density operator for the $3d$ states is defined by

$$\rho_{\mathbf{q}\lambda m\sigma} = \sqrt{\frac{2}{N}}\sum_{\mathbf{k}} A^{\dagger}_{\mathbf{k}+\mathbf{q}\lambda m\sigma}A_{\mathbf{k}\lambda m\sigma} \quad \text{with } \lambda = 1,2, \tag{19}$$

where $\mathbf{k}$ runs over the magnetic first BZ. The momentum conservation requires the relation $\mathbf{q}=\mathbf{q}_i-\mathbf{q}_f$. In Eq. (17), superscripts + and − stand for the backward and outward time legs, respectively.[23] Confining our discussion to the zero temperature, we take the average over the ground state. Therefore, Y^{+-} is nothing but a conventional correlation function in the equilibrium state.

The solid lines represent the bare Green's functions for the $4p$ electron and for the core hole. In the outward time leg, they are defined by $G^{(0)}_{4p}(\mathbf{k},t)=-i\langle T(p'_{\mathbf{k}}(t)p'^{\dagger}_{\mathbf{k}}(0)\ \rangle$ and $G^{(0)}_{1s}(\mathbf{k},t)=-i\langle T(s_{\mathbf{k}}(t)s^{\dagger}_{\mathbf{k}}(0)\ \rangle$. Then, the product of Green's functions $G^{(0)}_{4p}(\mathbf{p},-t)G^{(0)}_{1s}(\mathbf{p}-\mathbf{q}_i,\ t-\tau))G^{(0)}_{1s}(\mathbf{p}-\mathbf{q}_f,\tau)$ on the top half gives rise to a factor $\exp[i(\epsilon^{\eta}_{4p}(\mathbf{p})-\epsilon_{1s}-i\Gamma_{1s}-\omega_i)t]$, where Γ_{1s} is a lifetime broadening width of the $1s$ core hole. A similar argument is applied on the backward time leg, leading to a factor $\exp[-i(\epsilon^{\eta}_{4p}(\mathbf{p})-\epsilon_{1s}+i\Gamma_{1s}-\omega_i)(t'-u')]$. The Keldysh-Green function defined by Eq. (17) brings the time-dependent factor $e^{i\omega\tau}$ to the outward time leg and $e^{-i\omega\tau'}$ to the backward time leg. Noting that the core-hole potential works only in intervals $[t,0]$ and $[t',u']$, we integrate the time factor combined to the above product of Green's functions with respect to τ and t in the region of $t<\tau<0$, $-\infty<t<0$. The result is

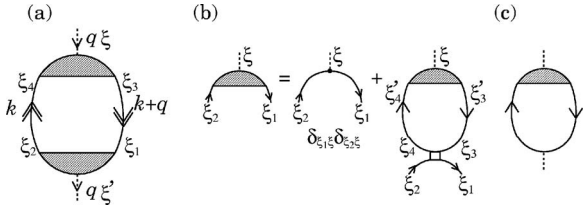

FIG. 8. (a) Diagrams for $Y^{+-}(q)$. Solid lines with double arrows are not the time-ordered Green's functions but the Keldysh-type ones connecting the outward time leg with the backward time leg. (b)Vertex function $\Lambda(q)$ within the RPA. Solid lines with arrows are the conventional time-ordered Green's functions. The square represents the four-point vertex of the $3d$ Coulomb interaction effective only at the same Ni sites. (c) Diagrams for the time-ordered $Y^{T}(q)$ within the RPA.

$$L^{\eta}_{B}(\omega_i;\omega) \equiv -\frac{V}{N}\int_{-\infty}^{0} dt\sum_{\mathbf{p}} \exp[i(\epsilon^{\eta}_{4p}(\mathbf{p}) - \epsilon_{1s} - i\Gamma_{1s} - \omega_i)t]\int_{t}^{0} d\tau e^{i\omega\tau}$$

$$= \frac{V}{N}\int \frac{\rho^{\eta}_{4p}(\epsilon)d\epsilon}{(\omega_i+\epsilon_{1s}+i\Gamma_{1s}-\epsilon)(\omega_i-\omega+\epsilon_{1s}+i\Gamma_{1s}-\epsilon)}, \tag{20}$$

where the sum over $4p$ states is replaced by the integration of the $4p$ DOS projected onto the η $(=x,y,z)$ symmetry, $\rho^{\eta}_{4p}(\epsilon)$. A similar factor has been derived in third-order perturbation theory by Abbamonte *et al.*[24] The integration with respect to τ' and t' in the backward time leg gives the term complex conjugate to Eq. (20). The integration with respect to u' gives the energy conservation factor, which guarantees that ω in Eq. (20) is the energy loss, $\omega=\omega_i-\omega_f$. Finally, combining these relations together, we obtain an expression of the RIXS intensity for the incident photon with the momentum and energy $q_i=(\mathbf{q}_i,\omega_i)$, polarization $e^{(\alpha_i)}$, and the scattered photon with the momentum and energy $q_f=(\mathbf{q}_f,\omega_f)$, polarization $e^{(\alpha_f)}$,

$$W(q_i,\alpha_i;q_f,\alpha_f) = \frac{|w|^4}{4\omega_i\omega_f}\frac{N}{2}\sum_{\xi\xi'} Y^{+-}_{\xi\xi'}(q)\left|\sum_{\eta} e^{(\alpha_i)}_{\eta}L^{\eta}_{B}(\omega_i;\omega)e^{(\alpha_f)}_{\eta}\right|^2, \tag{21}$$

where $q=q_i-q_f$.

B. Correlation function

We consider diagrams where one electron-hole pair remains after the RIXS process, as shown in Fig. 8(a). We write $Y^{+-}_{\xi',\xi}(q)$ in the form,

$$Y^{+-}_{\xi',\xi}(q) = \sum_{\xi_1\xi_2\xi_3\xi_4} \Lambda^{*}_{\xi_1\xi_2,\xi'}(q)\Pi^{+-(0)}_{\xi_1\xi_2,\xi_3\xi_4}(q)\Lambda_{\xi_3\xi_4,\xi}(q), \tag{22}$$

with

$$\Pi^{+-(0)}_{\xi_1\xi_2,\xi_3\xi_4}(q) = 2\pi\frac{2}{N}\sum_{\mathbf{k}}\sum_{j,j'}\delta(\omega - E_{j'}(\mathbf{k}+\mathbf{q}) + E_j(\mathbf{k})) \times[1-n_{j'}(\mathbf{k}+\mathbf{q})]n_j(\mathbf{k})U_{\xi_1 j'}(\mathbf{k}+\mathbf{q}) \times U^*_{\xi_3 j'}(\mathbf{k}+\mathbf{q})U_{\xi_4 j}(\mathbf{k})U^*_{\xi_2 j}(\mathbf{k}), \quad (23)$$

where j and j' denote energy eigenstates. The δ function in $\Pi^{+-(0)}(q)$ indicates that the interband transition from the valence band to the conduction band gives rise to the RIXS intensity. Only the weight of $3d$ states in the bands contributes to the intensity. The vertex function is given by $\Lambda_{\xi_3\xi_4,\xi}(q)=\delta_{\xi_3,\xi_4}\delta_{\xi_4,\xi}$ in the lowest order. Within the RPA, it is calculated by collecting the ladder diagrams shown in Fig. 8(b). We obtain

$$\Lambda_{\xi_1\xi_2,\xi}(q) = [\hat{I} - \hat{\Gamma}\hat{F}^{--}(q)]^{-1}_{\xi_1\xi_2,\xi\xi}, \quad (24)$$

where $\hat{I}$ represents a unit matrix. The component of the matrix $\hat{F}^{--}(q)$ is given by the conventional time-ordered propagator

$$[\hat{F}^{--}(q)]_{\xi_1\xi_2,\xi_3\xi_4} = -i\frac{2}{N}\sum_{\mathbf{k}}\int\frac{dk_0}{2\pi}[\hat{G}(\mathbf{k},k_0)]_{\xi_4\xi_2}[\hat{G}(\mathbf{k}+\mathbf{q},k_0+\omega)]_{\xi_1\xi_3} = \frac{2}{N}\sum_{\mathbf{k}}U_{\xi_4 j}(\mathbf{k})U^*_{\xi_2 j}(\mathbf{k})U_{\xi_1 j'}(\mathbf{k}+\mathbf{q})U^*_{\xi_3 j'}(\mathbf{k}+\mathbf{q}) \times\left[\frac{n_j(\mathbf{k})[1-n_{j'}(\mathbf{k}+\mathbf{q})]}{\omega - E_{j'}(\mathbf{k}+\mathbf{q}) + E_j(\mathbf{k}) + i\delta} - \frac{n_{j'}(\mathbf{k}+\mathbf{q})[1-n_j(\mathbf{k})]}{\omega - E_{j'}(\mathbf{k}+\mathbf{q}) + E_j(\mathbf{k}) - i\delta}\right]. \quad (25)$$

The component of the matrix $\hat{\Gamma}$ is given by the four-point vertex, which is nonzero only for ξ_1, ξ_2, ξ_3, ξ_4 belonging to the *same* Ni site. Explicitly, it is given by

$$[\hat{\Gamma}]_{\xi_1\xi_2,\xi_3\xi_4} = \Gamma^{(0)}(\nu_1\nu_4;\nu_2\nu_3), \quad (26)$$

$\xi_1=\lambda\nu_1$, $\xi_2=\lambda\nu_2$, $\xi_3=\lambda\nu_3$, $\xi_4=\lambda\nu_4$ with $\lambda=1,2$, and, otherwise, it is zero.

As already pointed out, the Keldysh-type Green's function $Y^{+-}_{\xi',\xi}(q)$ is equivalent to the conventional correlation function. Therefore, it may be more convenient to analyze the function with the help of the conventional time-ordered Green's function,

$$Y^T_{\xi',\xi}(q) = -i\int\langle T[(\rho_{\mathbf{q}\lambda' m'\sigma'})^\dagger(t)\rho_{\mathbf{q}\lambda m\sigma}(0)]\rangle e^{i\omega t}dt, \quad (27)$$

with T being the time-ordering operator. Considering the diagrams shown in Figs. 8(b) and 8(c), it is expressed within the RPA as

$$Y^T_{\xi',\xi}(q) = \{\hat{F}^{--}(q)[\hat{I} - \hat{\Gamma}\hat{F}^{--}(q)]^{-1}\}_{\xi'\xi',\xi\xi}. \quad (28)$$

This expression leads to Eq. (22) with the help of the fluctuation-dissipation theorem,

$$\sum_{\xi'\xi}Y^{+-}_{\xi'\xi}(q) = -i\sum_{\xi'\xi}[Y^{T*}_{\xi'\xi}(q) - Y^T_{\xi\xi'}(q)] \quad \text{for } \omega>0. \quad (29)$$

To show this fact, we first rewrite Eq. (25) as

$$\hat{F}^{--}(q) = \hat{F}^{--}_1(q) + i\hat{F}^{--}_2(q), \quad (30)$$

where $\hat{F}^{--}_1(q)$ and $\hat{F}^{--}_2(q)$ are Hermitian matrices. Then, using the Hermitian property, we transform $Y^T_{\xi'\xi}(q)^*$ as

$$Y^T_{\xi'\xi}(q)^* = \{[I-(F^{--}_1(q) - iF^{--}_2(q))\Gamma]^{-1} \times[F^{--}_1(q) - iF^{--}_2(q)] \times[I-\Gamma(F^{--}_1(q) + iF^{--}_2(q))] \times[I-\Gamma(F^{--}_1(q) + iF^{--}_2(q))]^{-1}\}_{\xi\xi,\xi'\xi'}. \quad (31)$$

Combining the similar expression for $Y^T_{\xi\xi'}(q)$, we have

$$Y^{T*}_{\xi'\xi}(q) - Y^T_{\xi\xi'}(q) = \{[I-(F^{--}_1(q) - iF^{--}_2(q))\Gamma]^{-1}(-2i)[\hat{F}^{--}_2(q)] \times[I-\Gamma(F^{--}_1(q) + iF^{--}_2(q))]^{-1}\}_{\xi\xi,\xi'\xi'}. \quad (32)$$

Since $-2F^{--}_2(q)$ is equivalent to $\Pi^{(0)}(q)$ for $\omega>0$, the RXS intensity given by Eq. (33) through Eq. (29) is equivalent to the one given by Eq. (22).

Equation (28) may have poles for some frequencies below the energy continuum of an electron-hole pair. These bound states may be called as d-d excitations, and give rise to extra RIXS peaks. To analyze the problem, we rewrite Eq. (28) as

$$Y^T_{\xi',\xi}(q) = [\hat{F}^{--}(q)^{-1} - \hat{\Gamma}]^{-1}_{\xi'\xi',\xi\xi}, \quad (33)$$

where $\hat{F}^{--}(q)^{-1}$ becomes a Hermitian matrix when ω is below the energy continuum. Therefore, $\hat{F}^{--}(q)^{-1}-\hat{\Gamma}$ can be diagonalized by a unitary matrix. Let the diagonalized matrix have a zero component at $\omega=\omega_B(\mathbf{q})$ with the corresponding eigenvector $B_{\xi_1\xi_2}(\mathbf{q})$. Then, $Y^T_{\xi'\xi}(q)$ can be expanded around $\omega\sim\omega_B(\mathbf{q})$ as

$$Y^T_{\xi'\xi}(q) = \frac{C_{\xi'\xi}(\mathbf{q})}{\omega - \omega_B(\mathbf{q})}, \quad (34)$$

with

$$C_{\xi'\xi}(\mathbf{q}) = \frac{B_{\xi'\xi'}(\mathbf{q})B^*_{\xi\xi}(\mathbf{q})}{\sum_{\xi_1\xi_2\xi_3\xi_4}B^*_{\xi_1\xi_2}(\mathbf{q})\frac{\partial}{\partial\omega}[\hat{F}^{--}(\mathbf{q},\omega=\omega_B(\mathbf{q}))^{-1}]_{\xi_1\xi_2,\xi_3\xi_4}B_{\xi_3\xi_4}(\mathbf{q})}. \quad (35)$$

Substituting the right-hand side of Eq. (29) by this equation, we obtain

$$\sum_{\xi'\xi}Y^{+-}_{\xi'\xi}(q) = 2\pi\sum_{\xi'\xi}C_{\xi'\xi}(\mathbf{q})\delta(\omega-\omega_B(\mathbf{q})). \quad (36)$$

This relation is to be inserted into Eq. (21) for evaluating the RIXS spectra.

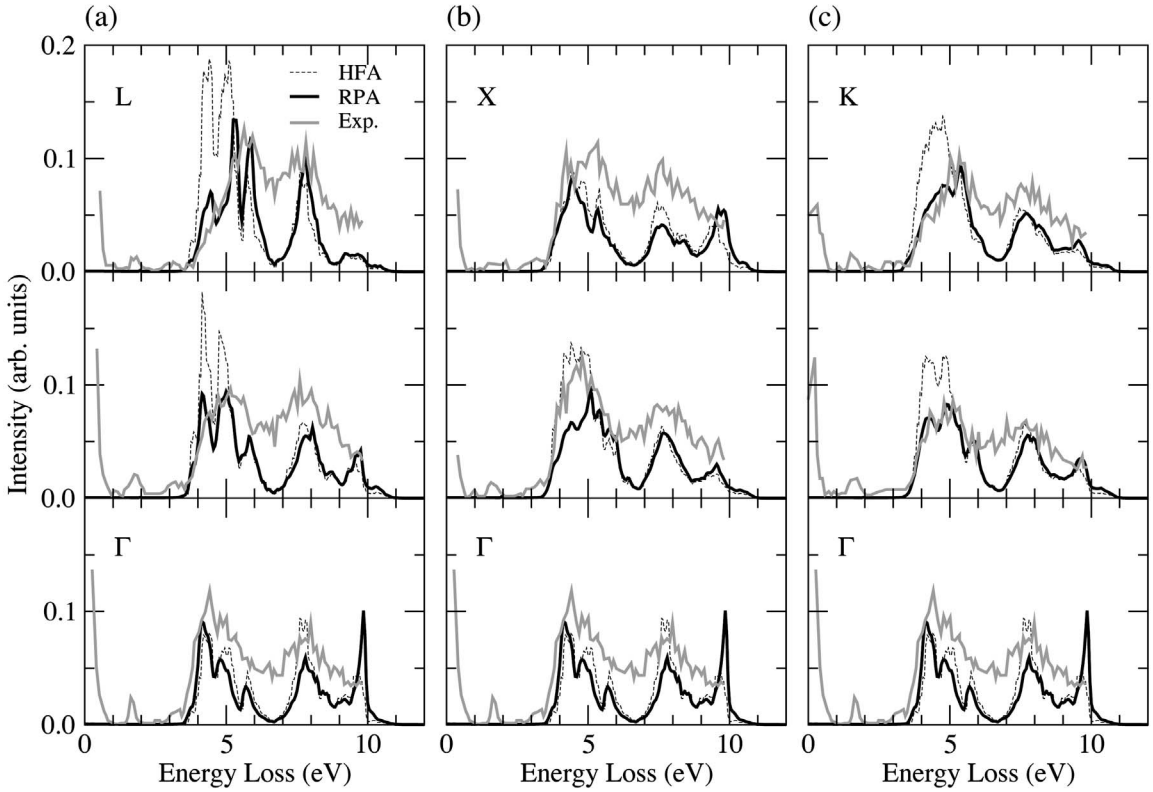

FIG. 9. RIXS spectra as a function of energy loss $\omega=\omega_i-\omega_f$, in comparison with the experiment by Ishii *et al.* (Ref. 10) Momentum transfer is along the symmetry lines: (a) $\Gamma-\frac{2\pi}{a}(0.25,0.25,0.25)-L$, (b) $\Gamma-\frac{2\pi}{a}(0.3,0,0)-X$, and (c) $\Gamma-\frac{2\pi}{a}(0.25,0.25,0)-K$. The incident photon energy is tuned to excite the $1s$ electron to the peak of the $4p$ DOS. The broken and solid lines are the results of the HFA and RPA, respectively. The dotted lines represent the experimental data (Ref. 10).

IV. CALCULATED RESULTS

We calculate the RIXS intensity from Eq. (21). In the experiment by Ishii *et al.*,[10] the incident photon energy is set to give the *K*-edge absorption peak, but the polarization of photon is not specified. Corresponding to the experiment, we use the $4p$ DOS obtained from the KKR band-structure calculation in the calculation of $L_B^{\eta}(\omega_i;\omega)$ [Eq. (20)], and tune the incident photon energy to excite the $1s$ electron on the peak of the $4p$ DOS. In the calculation of $Y^{+-}(q)$, we replace the δ function by the Lorentzian function with the FWHM $=0.2$ eV in order to take account of the instrumental resolution. Figure 9 shows the spectra, thus, calculated as a function of energy loss in comparison with the experiment, where the momentum transfer is chosen along symmetry lines in the BZ.

The experimental RIXS spectra below $\omega<9$ eV are roughly made up of two broad peaks, one of which is located around $\omega=4-6$ eV and another is around $\omega=8$ eV. In the HFA, we obtain peaks around $\omega=4-6$ eV and $\omega=8$ eV, which correspond to the experimental ones. In addition, we find an extra peak around the upper edge of the continuum spectra, ~ 10 eV, which is not confirmed by the experiment (the observation is limited below 10 eV). According to Eq. (23), the spectra are given by the excitation from the valence band to the conduction band. Only the weights of the $3d$ states contribute. In addition, as is clear from Eq. (16), the excited electron and hole by the core-hole potential have the same $3d$ orbital and spin indices. As shown in Figs. 5 and 6, the unoccupied states are concentrated in the minority spin states with the e_g character. Therefore, e_g DOS around 0–2 eV below the top of the valence band in the minority spin state may be responsible to the RIXS peak around $\omega=4-6$ eV, and the DOS around 3–4 eV below the top of the valence band may be responsible to the peak around $\omega=8$ eV. This interpretation roughly explains the RIXS spectra on the whole.

As regards the momentum dependence, the shape around $\omega=4-6$ eV considerably changes while that around 8 eV changes little with changing momenta from the Γ point to the

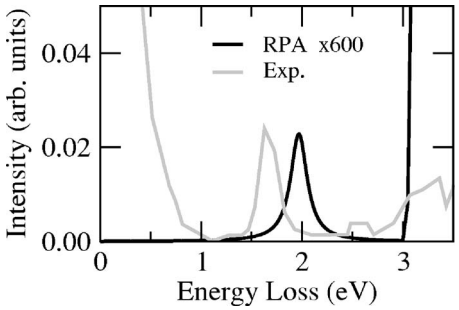

FIG. 10. RIXS intensity below the lower edge of the continuum at Γ point in comparison with the experiment (Ref 10). The calculated intensity is enlarged by multiplying 600 to make the spectra visible.

zone boundary in the experiment. In order to explain such behavior, we need to go beyond the HFA. We take account of the RPA correction, which enhances the intersite correlation of Ni atoms. We find that the intensities around 4–5 eV (excluding 5–6 eV) is strongly suppressed near the zone boundary, and thereby the peak position looks moving with changing momenta. This behavior does not mean the dispersion of some mode like a bound exciton but may be simply interpreted as changing weights with changing momenta in the continuum spectra. This reminds us of the RIXS spectra in La_2CuO_4, where the peak around $\omega=2$ eV shows considerable momentum dependence;[25] the peak is strongly suppressed near the zone boundary. We have reproduced well the spectral change by taking account of the RPA correction.[12] We also find that the RPA corrections are small on the peak around 8 eV, which changes little with changing momenta. These characteristics are the same along the three symmetry lines. Taking into consideration that the adjustable parameter is only the value of F^0, we could say that the spectral shapes show good agreement with the experiment.[10] Note that the sharp peak around $\omega=10$ eV is strongly suppressed with deviating momenta from the Γ point. This intensity is caused by the excitation due to the transition from the occupied e_g states around −6 eV to the unoccupied e_g states around 3 eV in the minority spin state and is enhanced by the RPA correlation only around the Γ point.

Below the lower edge of the continuum spectra, we obtain a bound state at $\omega=2$ eV, as shown in Fig. 10. The peak shows little momentum dependence, indicating that the bound state is well localized at a single Ni atom. This may be compared with the experimental peak at 1.7 eV, but the calculated intensity is about 2 orders of magnitude smaller than the experiment. At present, we do not know the real origin for this discrepancy.

V. CONCLUDING REMARKS

We have analyzed the RIXS spectra in NiO by developing the formalism of Nomura and Igarashi. This is based on the Keldysh-Green function formalism and relates the RIXS spectra to the density-density correlation function under the Born approximation to the core-hole potential. The use of the Born approximation had been justified for the RIXS in La_2CuO_4 by evaluating the multiple scattering effects.[14] Since NiO has a larger energy gap than La_2CuO_4, we expect that the Born approximation is better justified in NiO. We have introduced the tight-binding model including all the Ni $3d$ and O $2p$ orbitals, as well as the full Coulomb interaction between $3d$ orbitals, and have calculated the single-particle excitation within the HFA. The value of F^0 is adjusted to give the experimental energy gap in the single-particle excitation.

The electron correlation is expected to modify the single-particle energy bands given by the HFA.[26] According to the three-body scattering theory by the present authors,[27] one effect is the reduction of the energy gap from the HFA value. Since the value of F^0 is adjusted to give the experimental energy gap within the HFA, the present HFA is regarded as partly taking into account the correlation effect by using the effective value of F^0. Another prominent effect is that a "satellite" peak is created around 9 eV below the top of the valence band. The other is that the $3d$ states are pushed to upper energy position as a countereffect of the satellite creation. These modifications are limited to the deep states around the bottom of the valence band, mostly with the majority spin states. The RIXS spectra arise from an electron-hole pair excitation mainly in the minority spin channel. For the RIXS spectra with relatively low-energy loss values $\omega < 8$ eV, valence electrons around the bottom of the valence band have little contribution, and, therefore, the large modification of the single-particle excitation around the bottom of the valence band by the electron correlation may have little influence.

We have calculated the RIXS spectra using the single-particle band, thus, evaluated together with the $4p$ DOS by the LDA. The RIXS spectra arise from the band-to-band transition to screen the $1s$ core hole. We have obtained several peaks in the continuum spectra. Two peaks are found prominent around 4–6 and 8 eV. We have interpreted the origin of these peaks in terms of the e_g DOS. It is found that the RPA correction causes a suppression of the intensity around $\omega=4-5$ eV with momenta approaching to the zone boundary, by enhancing the intersite correlations of Ni atoms. Note that the similar behavior of RIXS spectra was found in La_2CuO_4 and that the same analysis has worked well. For NiO, we have obtained quantitative agreement with the experiment. We emphasize that the adjustable parameter is only the value of F^0 to give the experimental energy gap in the single-particle excitation. The good agreement with the experiment suggests that the present scheme is useful to analyze the RIXS spectra.

As regards the *d-d* excitation, we have obtained a bound state below the lower edge of the continuum spectrum. Its spectrum shows little momentum dependence, indicating that it is well localized at a single Ni sites. The peak position has been found close to the experimental one. However, the intensity is about 2 orders of magnitude smaller than the experimental one. The presence of crystal distortion might enhance the intensity of *d-d* excitation. At any rate, the real reason for this discrepancy is not known.

ACKNOWLEDGMENTS

We would like to thank H. Ishii for providing us with the experimental data prior to the publication and for valuable discussions. This work was partially supported by a Grant-in-Aid for Scientific Research from the Ministry of Education, Culture, Sports, Science, and Technology, Japan.

[1] S. Uchida, T. Ido, H. Takagi, T. Arima, Y. Tokura, and S. Tajima, Phys. Rev. B **43**, 7942 (1991).
[2] Y. Y. Wang, F. C. Zhang, V. P. Dravid, K. K. Ng, M. V. Klein, S. E. Schnatterly, and L. L. Miller, Phys. Rev. Lett. **77**, 1809 (1996).
[3] C.-C. Kao, W. A. L. Caliebe, J. Hastings, and J.-M. Gillet, Phys. Rev. B **54**, 16361 (1996).
[4] J. Hill, C.-C. Kao, W. Caliebe, M. Matsubara, A. Kotani, J. Peng, and R. Greene, Phys. Rev. Lett. **80**, 4967 (1998).
[5] M. Hasan, E. Isaacs, Z.-X. Shen, L. L. Miller, L. Tsutsui, T. Tohyama, and S. Maekawa, Science **288**, 1811 (2000).
[6] Y. J. Kim, J. P. Hill, C. A. Burns, S. Wakimoto, R. J. Birgeneau, D. Casa, T. Gog, and C. T. Venkataraman, Phys. Rev. Lett. **89**, 177003 (2002).
[7] T. Inami, T. Fukuda, J. Mizuki, S. Ishihara, H. Kondo, H. Nakao, T. Matsumura, K. Hirota, Y. Murakami, S. Maekawa *et al.*, Phys. Rev. B **67**, 045108 (2003).
[8] Y. J. Kim, J. P. Hill, H. Benthien, F. H. L. Essler, E. Jeckelmann, H. S. Choi, T. W. Noh, N. Motoyama, K. M. Kojima, S. Uchida *et al.*, Phys. Rev. Lett. **92**, 137402 (2004a).
[9] S. Suga, S. Imada, A. Higashiya, A. Shigemoto, S. Kasai, M. Sing, H. Fujiwara, A. Sekiyama, A. Yamasaki, C. Kim *et al.*, Phys. Rev. B **72**, 081101(R) (2005).
[10] H. Ishii (private communication).
[11] T. Nomura and J. Igarashi, J. Phys. Soc. Jpn. **73**, 1677 (2004).
[12] T. Nomura and J. I. Igarashi, Phys. Rev. B **71**, 035110 (2005).
[13] P. Nozières and E. Abrahams, Phys. Rev. B **10**, 3099 (1974).
[14] J. I. Igarashi, T. Nomura, and M. Takahashi, Phys. Rev. B **74**, 245122 (2006).
[15] W. L. Roth, Phys. Rev. **110**, 1333 (1958).
[16] G. A. Sawatzky and J. W. Allen, Phys. Rev. Lett. **53**, 2339 (1984).
[17] W. Neubeck, C. Vettier, F. de Bergevin, F. Yakhou, D. Mannix, O. Bengone, M. Alouani, and A. Barbier, Phys. Rev. B **63**, 134430 (2001).
[18] J. C. Slater and G. F. Koster, Phys. Rev. **94**, 1498 (1954).
[19] T. Mizokawa and A. Fujimori, Phys. Rev. B **53**, R4201 (1996).
[20] J. van Elp, H. Eskes, P. Kuiper, and G. A. Sawatzky, Phys. Rev. B **45**, 1612 (1992).
[21] L. F. Mattheiss, Phys. Rev. B **5**, 290 (1972).
[22] L. V. Keldysh, Sov. Phys. JETP **20**, 1018 (1965).
[23] L. D. Landau and E. M. Lifshitz, *Physical Kinetics* (Butterworth-Heinemann, Oxford, 1962), Chap. 10.
[24] P. Abbamonte, C. A. Burns, E. D. Isaacs, P. M. Platzman, L. L. Miller, S. W. Cheong, and M. V. Klein, Phys. Rev. Lett. **83**, 860 (1999).
[25] Y. J. Kim, J. P. Hill, S. Komiya, Y. Ando, D. Casa, T. Gog, and C. T. Venkataraman, Phys. Rev. B **70**, 094524 (2004).
[26] M. Imada, A. Fujimori, and Y. Tokura, Rev. Mod. Phys. **70**, 1039 (1998).
[27] M. Takahashi and J. I. Igarashi, Phys. Rev. B **54**, 13566 (1996).